Int J Adv Manuf Technol (2017) 92:789–802
DOI 10.1007/s00170-017-0177-5

ORIGINAL ARTICLE

Generation of consistent skin model shape based on FEA method

Xingyu Yan[1] · **Alex Ballu**[1]

Received: 18 October 2016 / Accepted: 16 February 2017 / Published online: 3 March 2017

Abstract Controlling product geometric quality is an important issue, because real parts deviate from their nominal value (e.g., in form, orientation, and position error of features, size of part, etc.). To analyze the influence of these deviations on final product, one solution is to consider the nonnominal Skin Model Shape to simulate assembly, manufacturing, or metrology. The modeling of nonnominal parts is still in its initial phases. First, methods of generating a single feature with deviations are reviewed and classified. With the combination of the single nonideal features to obtain the complete nonideal model of the part, geometrical issues appear, such as gaps and self-intersections. These can be influenced by acute and obtuse angles and the ratio between mesh size and deviation value. From an analysis of these issues, two deviation combination methods are proposed to preserve the manufacturing deviation of features and consistency of the model. These methods are qualified as local and global methods. The local method is based on the iterative calculation of mesh regularization. The global method is based on finite element analysis, with manufacturing deviations added to the nominal model by the penalty function approach. The effectiveness and efficiency of both kinds of method are compared on a trial geometry. The global method is preferred as it needs no iterative calculation, no stop criteria and gives better results. Finally, the proposed method is validated on a more complex mechanical part: a cutter body.

Keywords Computer-Aided Tolerancing · Manufacturing deviation · Skin model shape · Random field · Finite element analysis

✉ Alex Ballu
alex.ballu@u-bordeaux.fr

[1] Universite de Bordeaux, I2M, UMR 5295, F-33400 Talence, France

1 Introduction

The geometrical quality of a product, one of the qualities that is of concern from the design stage through to manufacturing, influences the final product function and reliability and draws a lot of research attention. To predict the potential problems caused by geometrical uncertainties during the manufacturing process and to increase the robustness of product design, based on Computer-Aided Design (CAD) systems, several models have been proposed to express tolerances and conduct tolerance analysis [1, 2].

To model tolerances, offset zones [3] are introduced to represent the tolerance zones by offsetting the boundary of the nominal model. A vectorial approach [4] is proposed to conduct tolerance analysis [5]. In the work of Desrochers et al. [6], the Technologically and Topologically Related Surfaces (TTRS) method is developed, which allows for the integration of tolerance information into a CAD system. Meanwhile, simulation based on Small Displacement Torsor (SDT) [7], Proportioned Assembly Clearance Volume (PACV) [8], polytopes [9], and Tolerance Map (T-Map) [10] have all been developed. Some of these models have been integrated into the CAD system or implemented in Computer-Aided Tolerancing (CAT) software.

While form error (detailed shape defect) influences various stages of manufacturing and assembly, the current models used for tolerance simulation are usually based on simplified variations (orientation and location) of the nominal model [11, 12], which cannot represent the real product. Meanwhile, the expression of tolerance specifications based on the nominal model leads to ambiguities [13] and may cause dysfunctions.

Given the limitations of nominal model-based methods, many other models have been developed which could represent detailed geometric deviations. In the work of Hu et al. [14], random rough surfaces are simulated by Fourier analysis,

and the contact area of the rough surface is simulated by Yastrebov et al. [15]. A manufacturing signature which contains shape error is considered in contact simulation by Wilma et al. [16]. In the work of Cao et al. [17], a surface with multiscale deviation is simulated and evaluated with tolerance specification. Surfaces with form deviations are also simulated for compliant sheet metal assembly [18, 19] to optimize the assembly sequence or locating methods. Besides the models mentioned above, in order to express shape defects and specifications, Ballu and Mathieu propose the Skin Model [20]. As the basic concept of the Geometrical Product Specification (GPS) standard [21], the Skin Model is a nonideal model representing the actual shape of real parts, which can be very different from the nominal model. With this model, various kinds of geometrical deviation can be expressed. However, as the Skin Model is an infinite description of a real part, it is impossible to integrate it into computer software to conduct geometric defect simulation, assembly simulation, etc. The skin model shape is proposed by Anwer et al. [22, 23] to indicate a specific Skin Model which could be described with finite parameters in the software.

In the different stages of the product lifecycle, there could be different purposes and methods for generating skin model shapes. In the design stage, when only a nominal model is available, skin model shapes could be generated by simulation methods [24], while in the later stages, they could be generated from the simulation results of the manufacturing process, or even from measuring actual parts [25].

To be more realistic, the simulation is applied independently to each feature of the part or to each group of features; this enables location errors to be introduced according to the manufacturing process and part setup. By doing this, geometric inconsistencies appear at the edges when the whole part surface is reconstructed from the individual ones. The objective of this paper is to present the geometric issues involved when combining the individual features and to propose a method to obtain fully consistent skin model shapes for any kind of surface.

In the first part, different approaches for form error simulation are reviewed. Next, the geometrical issues of combining these surfaces are described. From the issues, different methods are proposed, and particularly a method based on finite element analysis (FEA). Finally, the method is applied to a trial part and to a representative part from the mechanical industry.

2 Simulation methods for skin model shape

Unlike the nominal CAD model, the Skin Model is defined as a nonideal model which could represent the imperfect shape of a real part. The simulation and visualization of a Skin Model could help engineers better understand any potential manufacturing defects and assist them in making the appropriate decisions. Due to the imperfect shape of the Skin Model, its application could be extended to many other areas, such as tolerance analysis and virtual metrology.

With the increasing demands on manufacturing precision, the simulation and application of the Skin Model have drawn a lot of research interest in recent years. Due to its inherent nonideal character, a discrete representation is more suitable for Skin Model simulation [24]. Meanwhile, most Computer-Aided Engineering (CAE) or Computer-Aided Manufacturing (CAM) tools, like FEA, and measurement data are based on the discrete assumption. In this context, the discrete representation of the Skin Model will be of benefit to the reuse of data from manufacturing process simulation or measurement, which leads in turn to a more realistic simulation result. Thus, in earlier studies, to implement the Skin Model concept into computer software, the skin model shape is introduced as a specific discrete instance of Skin Model [23, 26].

The simulation of manufacturing defects is conducted before applying the skin model shape to various applications. Due to the different mechanisms in the various manufacturing processes, the parts tend to have distinct geometric defect patterns after different machining processes. As CAE and CAM methods have developed, many studies have been done to simulate the manufacturing processes and results. In the work of Wang et al. [27], FEA is used to simulate the stamping process and provide data to optimize the forming process. Simulation of the welding process considering nonideal compliant parts and locating deviation is studied by Hu et al. [28], who estimate the dimensional deviation of final assembly. Virtual machining, looking at the relation between workpiece, machining tool, and machining process, has drawn a great deal of research attention during recent decades [29–34]. Altintas et al. [35] provide a detailed review of virtual machining simulation methods and classify them into five categories, depending on the simulation principles: solid model-based; wire frame-based; voxel-, dexel-, and z-buffer-based; point-based; and analytical methods.

The simulation methods mentioned above are process-oriented and deal mainly with specific manufacturing processes, in order to predict and optimize the parameters, such as cutting force, torque, and tool path. The more detailed structures and factors that are considered during the simulation, the more calculation resources, and time will be required.

To simulate the skin model shape, only the final part with manufacturing defect is used. General and geometry-oriented simulation methods, which aim at producing a part with manufacturing defects rather than an analysis of the manufacturing process, are also studied. Based on the principles of these methods, they are

Table 1 Geometry-oriented manufacturing defect simulation methods

Category		Methods
Random noise		1D/3D random noise [36]
Mesh morphing		Random shapes [18, 37]
		Second-order shapes [24]
Modal-based methods	Without training sets	Zernike polynomials [40]
		Random field [23]
		Discrete cosine transform [16, 19]
		Natural vibration mode [17, 39]
	With training sets	Principal component analysis [25]

classified into three categories, which are random noise, mesh morphing, and modal-based methods. In the work of Zhang et al. [36], both 1D and 3D random noise are used to generate random local deviations. Mesh morphing-based methods are introduced to simulate random and systematic manufacturing defects [18, 24, 37]. Modal-based methods simulate surface defects by linear combination of form error modes. Modes used in simulation can be sine or cosine terms, polynomials, or values from Eigen decompositions [16, 17, 19, 23, 38–40]. In addition, using several training sets (data sets used to generate mode bases), a principal component analysis (PCA)-based statistical shape analysis method could be used to generate skin model shapes [24]. Table 1 shows the classification of different methods.

Either process-oriented or geometry-oriented simulation methods could be used for the simulation of the skin model shape. Process-oriented methods could provide a more realistic simulation result, although they require more information about the product and the detailed manufacturing process. For the early design stage, when only limited product or manufacturing information is available, the geometry-oriented general simulation method is a good choice. Moreover, with appropriate control parameters, it is possible to simulate a realistic skin model shape by geometry-oriented methods. In the next section, the geometry-oriented general simulation methods are applied.

Concerning the general geometry-oriented simulation methods, all the form error simulation approaches may be applied to simple canonic surfaces (plane, cylinder, sphere, and torus). Some of them may be applied to a set of canonic surfaces or to the whole surface of a complex part: 3D random noise and morphing. However, on an actual workpiece, particularly on a machined workpiece, there are independencies between isolated features or groups of fixtures due to specific machining conditions and clamping positions; different clamping positions introduce orientation and position errors. To simulate such errors, local independent simulations on features are required. After the independent simulations, the generated surfaces must be combined to create the skin model shape.

In [26], Schleich et al. proposed a skin model shape simulation process. At first, the tessellated model is generated from the nominal model, and then partition operation is conducted to acquire independent features. For each feature, different kinds of deviations are simulated, and they are added to the discrete nominal model directly to generate the skin model shapes.

In our study, we use a different method and treat each feature independently, emphasizing feature segmentation and combination processes [41]. Simulation of the skin model shape is divided into three steps, as described below:

- Segmentation. To be able to treat each feature independently and simulate deviations with different precision requirements, segmentation of the feature is conducted in advance.
- Manufacturing deviation simulation. Geometric manufacturing defects on the skin model shape are simulated. They are saved as deviation data for each vertex.
- Deviation combination. When the geometric deviations are simulated, they are combined and added to the original nominal model.

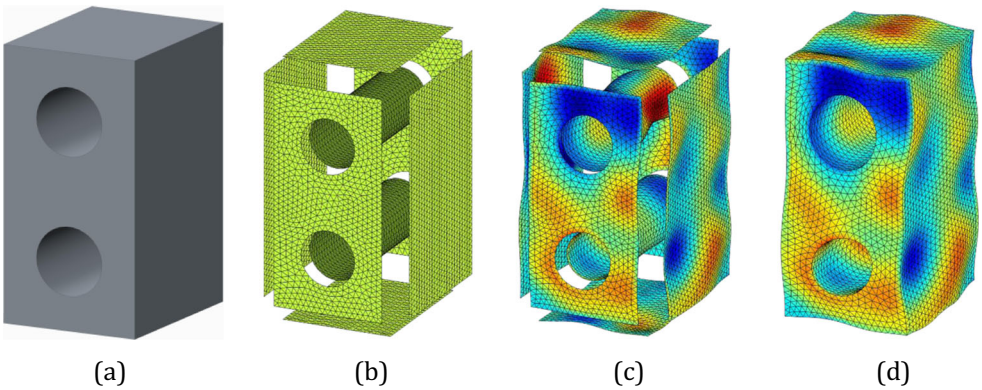

Fig. 1 Process for the generation of the skin model shapes. **a** Nominal model of the part. **b** Discretization and segmentation of the nominal model. **c** Simulate manufacturing deviations on each feature. **d** Combine all deviation data and nominal model into a complete skin model shape

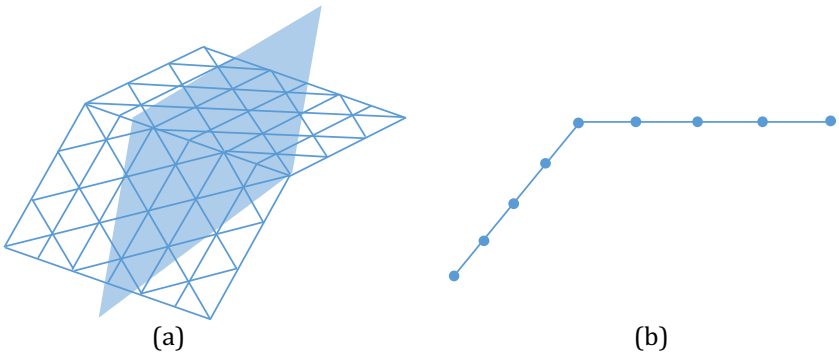

Fig. 2 Examples of connected features. **a** Two connected mesh planes and the section plane in 3D. **b** 2D section view

Figure 1 shows the simulation result at each step. As the deviations are simulated independently for each feature, and as the corresponding features have connections at their boundaries, combining the independent deviation data is a problem. In the following, geometric issues that appear during deviation combination are studied and requirements for deviation combination are summarized. Next, local and global solutions are proposed to handle these geometric issues.

3 Geometric issues

This section highlights the difficulties encountered in combining deviation data from each feature and adding them to the nominal model. The following sections are illustrated with 2D examples, as in Fig. 2b (assume the vertices lie in the same section plane), but they are representative of the main problems in 3D space.

The vertex normal is estimated by mean weighted equally algorithm [42]. Figure 3 shows the difference when we consider each feature independently or not. To simulate manufacturing deviation, which has independence between features, the situation in Fig. 3b is closer to reality. Thus, in what follows in this paper, the vertex normal is estimated for single features after segmentation, as shown in Fig. 3b.

3.1 Nonconnection

Unlike the features in the nominal model, which are connected at the edges, independent features with form deviations are no longer connected when we put them together. Figure 4 shows 2D sections and a 3D model of two intersecting planes. The nominal model is shown in Fig. 4a, where dashed lines represent a section view of two connected planes without form error, circles or squares in the dashed lines represent vertices on the faces, and the two faces are connected at the corner vertex. Assuming that the deviation of vertices outside the model is positive (+) and inside the model is negative (−), there are four types of configuration for the corner vertex, which can be seen in Fig. 4b. Solid lines, circles, and squares represent the section view of features with form error. One can imagine intersections between neighboring surfaces, but Fig. 4b illustrates cases without intersection.

As can be seen from the figures, depending on the configuration type and deviation value, sometimes, the two features are not connected while sometimes they intersect. The 3D case is much more complex. Figure 5 illustrates on a 3D view the fact that the surfaces may have zones of connection and nonconnection on one and the same edge. To guarantee the topological coherence of skin model shape, this issue has to be resolved.

3.2 Face connection

It is possible to calculate the intersection between features and delete the intersect parts, or calculate the split and fill in more vertices. In [43–45], mesh repairing methods are developed. This is not easy to carry out and the topology of the mesh needs to be changed. Meanwhile, it leads to more problems, such as the deviation simulation of new added vertices, the choice of new edge or corner, etc. Thus, a simpler method is preferred.

The simplest way to connect the faces is to add the simulated deviation to the vertices of the nominal model (discrete but not segmented into separate features) directly. The deviations are added along the vertex normals. This makes a vertex on an edge, which belongs to two faces, has two deviations along the normal direction of the two faces at the vertex, and the final vertex is the

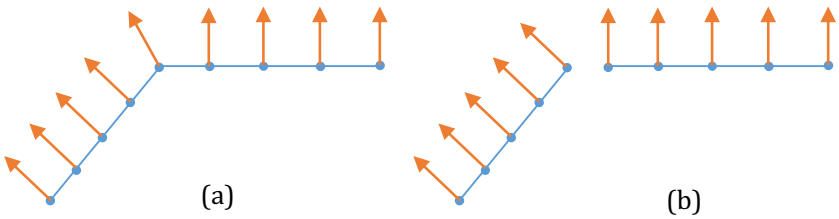

Fig. 3 Estimation of vertex normal. **a** Before feature segmentation. **b** after feature segmentation

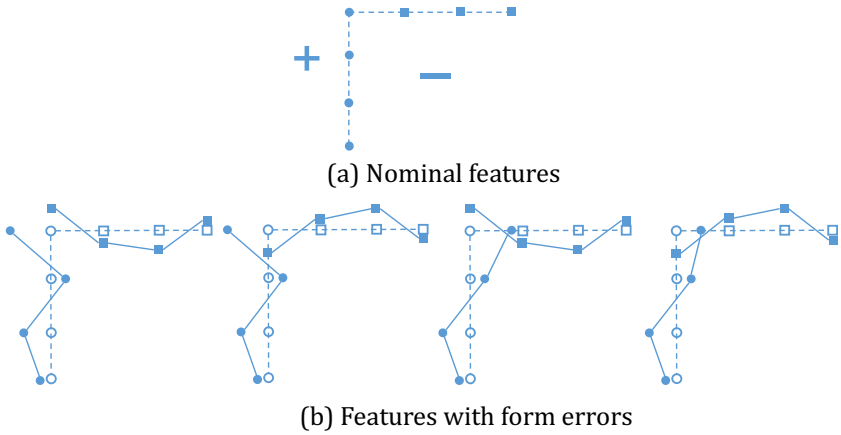

Fig. 4 Two connected features with and without form error

result of the addition of the two deviation vectors. Figure 6 shows an example of deviation addition on an edge vertex.

By applying this combination method, Fig. 7 shows the combination results of Fig. 4b and the results look appropriate for these configurations.

3.3 Obtuse and acute dihedral angles

However, when the connected features are at an obtuse or acute dihedral angle, there are new issues. The precision of each feature is influenced during the combination process by vector addition. Figure 8a shows the situation when two connected features are at an obtuse dihedral angle. By the principal of vector addition, the position of the edge vertex after combination can be easily calculated. However, this point does not correspond to the desired point. It is clear that by the addition of vectors, shape error for both single features is increased. For the acute dihedral angle in Fig. 8b, the deviation of the edge vertex decreases in a similar way.

The desired point is the intersection of two offset lines parallel to the two nominal lines; the two values of the offsets are equal to the two deviations of the edge vertex according to the two lines. Thus, the intersection point keeps the deviation of the edge vertex along the normal direction the same as before the deviation combination. In the proposed method, the objective will be to obtain this intersection point.

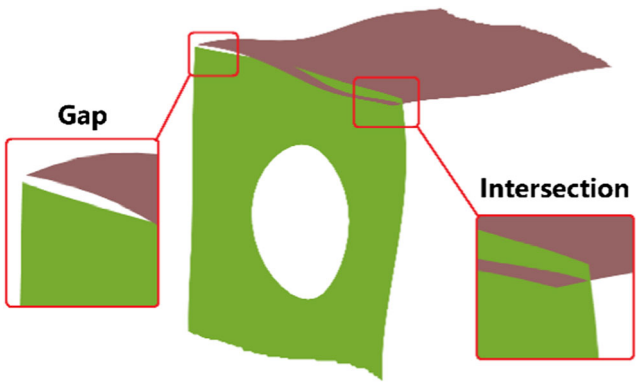

Fig. 5 3D view of the intersection and gap between features with form error

3.4 Ratio mesh size/deviation magnitude

The visualization of the form error shape is also important, as it could help engineers to understand potential defects of parts, make optimal decisions, and improve the manufacturing process [46]. Besides using the contour map of deviation, an amplified form error shape can show the deviation directly. Thus, we amplify the form errors on the skin model shape. However, this amplification also causes problems when a combination is conducted.

This is seen in Fig. 9. The amplified deviation may become larger than the mesh size, as shown in Fig. 9a. When the combination method is used by direct deviation addition to a nominal model, mesh triangles connected to the edge vertex will be overstretched or intersect with each other. Figure 9b shows the combination result with amplified deviation. These overstretching and intersection problems could also happen in precision simulation, when the mesh size is smaller than or close to deviation value.

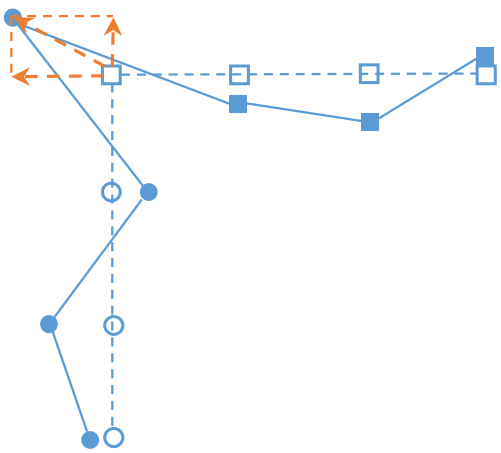

Fig. 6 Principle of deviation addition on nominal model directly

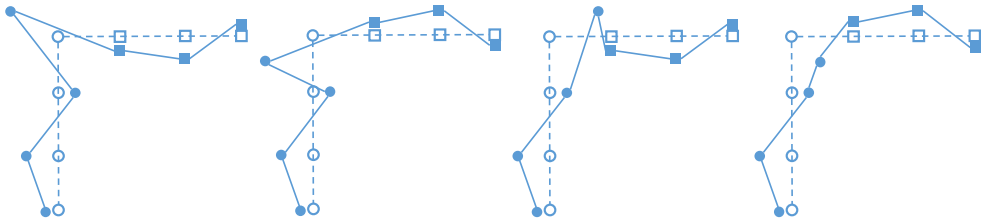

Fig. 7 Combination result by deviation addition on vertices of nominal model directly

4 Deviation combination methods

Several methods have been studied to combine the geometric deviations in a single mesh without intersection or stretching, while guaranteeing the precision of the feature. Based on their principles, they are classified as a local method or a global method.

4.1 Local method

In local methods, the deviations are first added to the nominal model, and then the mesh regularization process can be conducted to eliminate any intersection or split on the mesh [23]. The general process used for local methods is explained below:

- Computation of deviations for each feature independently.
- Addition of the deviations to the nominal model. For vertices inside the faces, the deviations are added along the normal direction directly. For vertices on the edges or corners, the positions of the vertices are calculated as the intersection of local tangent planes, as explained in Sect. 3.3.
- Regularization of the mesh to handle mesh problems with the skin model shape. Two methods are used, one based on Laplacian mesh regularization and the other on spring analogy. In local methods, regularization consists in moving each vertex only according to the neighboring ones.

Next, the principles of the two regularization methods are explained.

4.1.1 Laplacian mesh regularization

The Laplacian mesh regularization method [47], which is simple and fast, has been used to regularize the mesh in many different applications [48, 49].

Laplacian regularization is based on the umbrella operator [50] to adjust the position of the vertices of the mesh repeatedly. As explained in Fig. 10, the umbrella operator $U(P)$ of a vertex P is a vector, which is defined by the following expression:

$$U(P) = \frac{1}{\sum_i w_i} \sum_i w_i Q_i - P \tag{1}$$

where P is the vertex to be adjusted and Q_i are the neighbors of P. The w_i are positive weights which can be adjusted, but one simple way is to set $w_i = 1$. The position of vertex P is adjusted by adding a scaled umbrella operator (P):

$$P_{new} = P_{old} + \lambda \ U(P_{old}) \tag{2}$$

P_{ole} and P_{new} are the coordinates of vertex P before and after adjustment, $\lambda > 0$ is a small positive number. Every vertex coordinate is adjusted by iteration with Eq. 2, and parameter λ decides the adjustment speed in each iteration. The operator $U(P)$ can be decomposed according to the normal vector n and tangent vector t at vertex P, then:

$$P_{new} = P_{old} + \lambda_1 \ U_n(P_{old}) + \lambda_2 \ U_t(P_{old}) \tag{3}$$

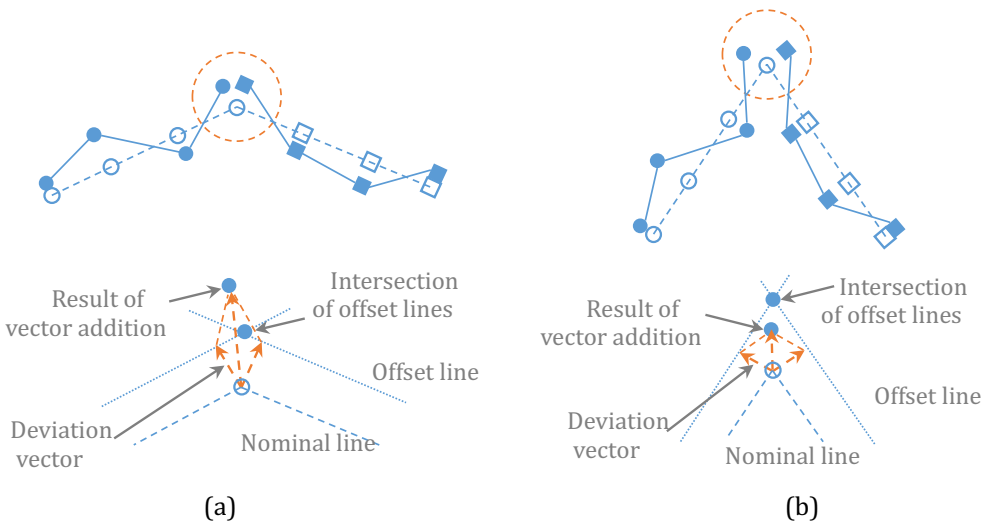

Fig. 8 Influence on precision of features of **a** obtuse dihedral angle and **b** acute dihedral angle

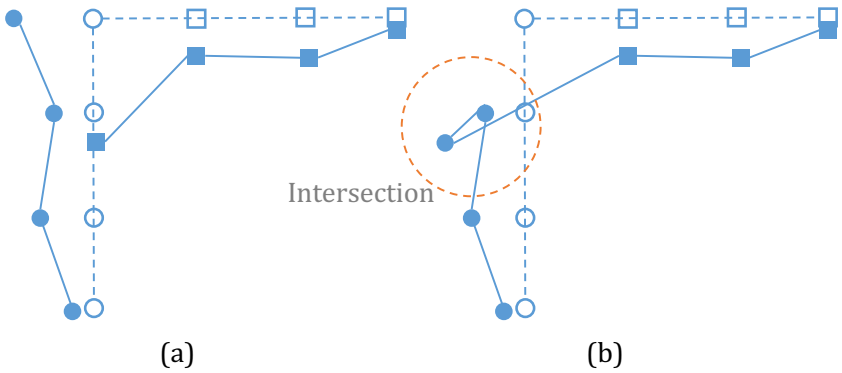

Fig. 9 Overstretch and intersection of mesh when deviation is larger than the mesh size

where $U_n(P)$ and $U_t(P)$ are the normal and tangential components of $U(P)$. By optimizing the calculation method of $U(P)$ and regularization speed λ, the method is improved by Ohtake et al. [47].

The Laplacian mesh regularization method is efficient and easy to apply. As shown in Eq. 3, it is possible to adjust the position of the vertices along a specific direction. Thus, to conserve the geometric precision of features, we adjust the vertices inside a surface only by the tangential component of the umbrella operator. This is illustrated in Fig. 11a, where vectors t and n correspond to the tangential and normal vectors, respectively. After mesh regularization, the manufacturing defects, which are expressed by the deviations along vertex normal directions, are not influenced.

For vertices on the edge, the umbrella operator is projected to a direction which is perpendicular to the two normals of the local tangent planes of vertex P. As explained in Fig. 11b, n_1 and n_2 are the normals of local tangent planes when vertex P is on the edge of two connected faces S_1 and S_2. Direction n_3 is perpendicular to both n_1 and n_2, thus adjustment along n_3 will not influence deviation along these two normal directions.

For vertices on the corner, they already have deviations along three nonparallel directions, thus their position will be fixed during the mesh regularization process.

4.1.2 Spring analogy

The spring analogy is commonly used in Computational Fluid Dynamics (CFD) for moving boundary problems and mesh regularization [51–53]. Due to its simple and basic assumption, modification of the mesh can be done efficiently.

Spring analogy applies Hook's law to adjust the mesh; the principle is explained in Fig. 12. Based on the definition of equilibrium length, the method can be classified into vertex springs and segment springs [52], and their equations are generalized. Let point P be the vertex to be adjusted, and Q_i its neighbor vertices, the force applied to vertex P is

$$F_P = \sum_i k_i(Q_i - P - d_i) \tag{4}$$

k_i is the stiffness of the spring, and d_i is the equilibrium vector. For vertex springs, the equilibrium vector is zero, while for segment springs, d_i is defined as:

$$d_i = Q_{i,old} - P_{old} \tag{5}$$

where the subscript "old" indicates the initial position of the vertices. The displacement vector of vertex P is

$$\delta_P = \frac{F_P}{\sum_i k_i} \tag{6}$$

By solving the equations iteratively, the position of the vertices can be calculated:

$$P_{new} = P_{new} + \delta_P \tag{7}$$

For vertex springs, if we set the stiffness $k_i = 1$, it is the same as the simplest umbrella-operator $U(P)$, which has been explained above. Both the vertex spring and segment spring methods can be improved by modifying the stiffness k_i.

As with the 2D spring analogy in its application to our problem, 3D springs are considered to calculate vertex displacement. Next, to conserve the geometric deviation

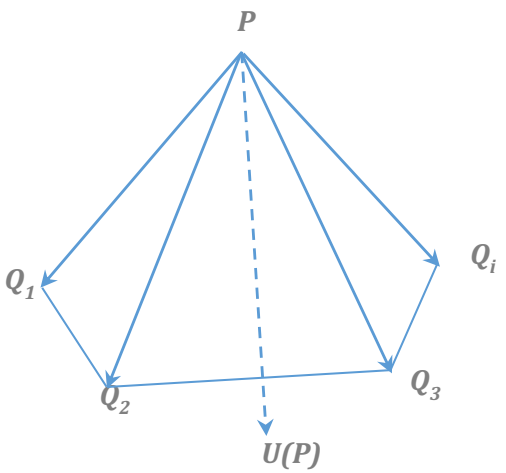

Fig. 10 Principle of the umbrella operator

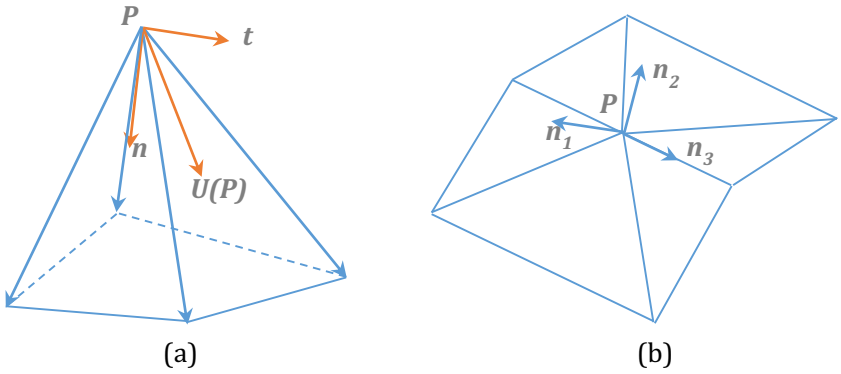

Fig. 11 Projection of umbrella operator during mesh regularization process

of the features, displacement δ_P is projected in a specific direction which is the same as in the Laplacian mesh regularization method.

4.1.3 2D example by local method

The example in Fig. 13 shows mesh regularization by spring analogy. Dashed lines indicate the nominal model, while solid lines indicate the model with deviations. Figure 13a shows the model before regularization, and Fig. 13b shows the model after regularization. As seen from Fig. 13b, vertices are adjusted only along their local tangent direction. The local mesh regularization method works in the same way for other situations, such as obtuse or acute dihedral angles.

4.2 Global method

In the local methods proposed above, the mesh is adjusted with certain direction constraints. Based on this principle, we propose another method to add direction constraints and solve the regularization problem globally.

In our combination and adjustment problem, where every vertex has at least one adjustment constraint, the method for adding constraints and solving equations efficiently is important. Finite element analysis (FEA) which has a standard solving process and can deal with complicated boundary problems is a promising way to solve the issue.

FEA is an efficient tool in structural design and analysis. It decomposes complex structures into small basic elements and provides a standard solving process. This benefits its implementation in computer programs, and complex structural problems are solved as simpler ones with the same process. In calculating CFD problems, where mesh is moving during simulation, FEA is also used for mesh regularization [54, 55].

With FEA, the 3D bar element is used to calculate the adjustment of vertex, which is similar to the spring in the spring analogy method. The penalty function approach is used to add adjustment direction constraints. The regularization problem defined by FEA is a linear problem, and the calculation only needs to be conducted once. The process of combination with FEA is shown below:

- Simulation of deviations on each feature independently. The deviation is not added to the vertex of the feature immediately, but stored as a displacement boundary constraint along the normal direction of the vertex.
- Generation of matrix for FEA based on the existing mesh model. Every edge of the mesh triangles is taken as a 3D bar element.
- Definition of the boundary displacement constraints corresponding to the deviations.
- Solving the FEA problem using the penalty function approach [56] to generate the regularized skin model shape.

In the following, the basic concept of FEA and the penalty function approach are introduced.

4.2.1 Finite element analysis

Typically, for a static FEA, the stiffness equation is applied to the considered elements:

$$K^e \cdot q^e = P^e \tag{8}$$

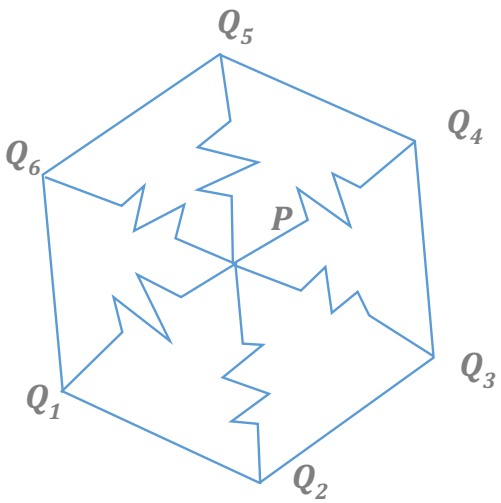

Fig. 12 Principle of Spring Analogy

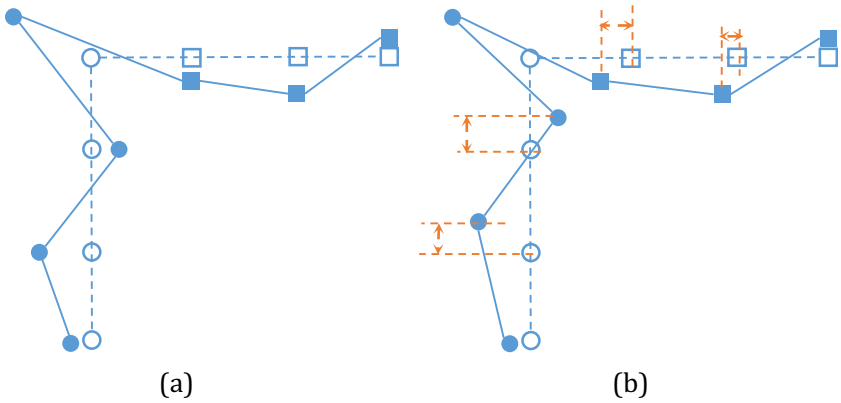

Fig. 13 2D mesh regularization example **a** before regularization and **b** after regularization

where K^e is the stiffness matrix, P^e is the nodal force vector, and q^e is the nodal displacement vector which needs to be solved for each element. They are defined in a local coordinate system associated with the corresponding element. To conduct the analysis and to solve the displacements of all the nodes in the structure, they should be transformed into a global coordinate system and assembled together. With the transformation matrix T^e, we obtain

$$\begin{cases} \bar{K^e} &= T^{eT} K^e T^e \\ \bar{P^e} &= T^{eT} P^e \\ q^e &= T^e \bar{q^e} \end{cases} \tag{9}$$

$\overline{K^e}$, $\overline{q^e}$, and $\overline{P^e}$ are the stiffness matrix, displacement vector, and force vector for elements in a global coordinate system, respectively. Once the displacement vector is calculated, other parameters (like strain, stress) can be solved based on their relation. For more detailed information about FEA, such as how to establish the stiffness equation and solve it, we refer readers to [56, 57].

4.2.2 Penalty function approach

To solve the stiffness equation with specified boundary conditions, there are several methods, such as direct solving, the Lagrange multiplier method, and the penalty function approach. As the penalty function approach keeps the structure of the original equations (matrix size, ranking, and symmetry), it reduces the complexity of large-scale computing dramatically and has been widely used in engineering applications. We apply this method to our mesh adjustment. The principle of the penalty function approach is shown below.

For a finite element model, its potential energy function Π is

$$\Pi = \frac{1}{2} q^T K q - F^T q \tag{10}$$

where q is the displacement vector of the system, K is the stiffness matrix, and F is the external force vector added to the nodes. To introduce the displacement boundary conditions, the displacement relation between coordinates can be written as

$$Cq = d \tag{11}$$

C is the matrix containing the displacement relations between the coordinates of the vertices, and d is the vector of displacement boundary conditions (corresponding to the simulated form deviations along normal directions in our case). A very large number S is introduced, modifying the potential energy function as:

$$\Pi^* = \frac{1}{2} q^T K q - F^T q + \frac{1}{2} S(Cq - d)^2 \tag{12}$$

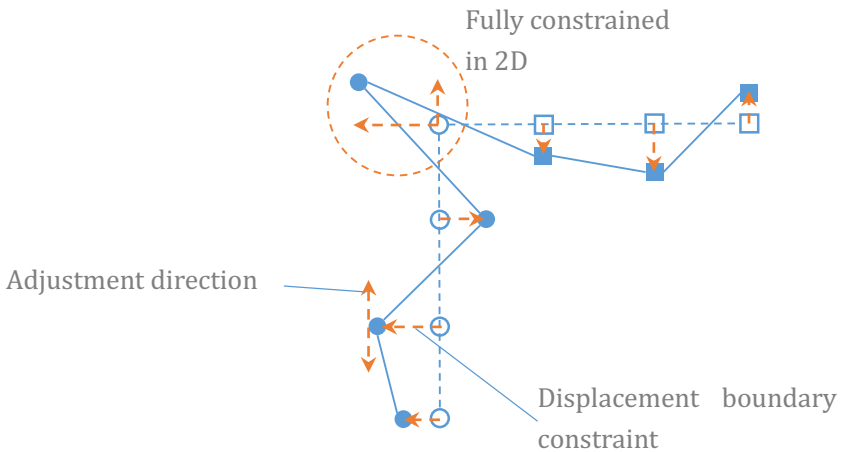

Fig. 14 Example of FEA-based mesh regularization method in 2D

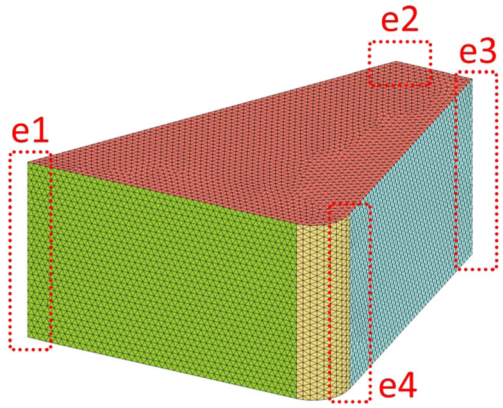

Fig. 15 Model used for simulation and comparison

Since S is a very large number, Π^* can take its minimum value only when $(Cq-d)\approx 0$ so that the displacement boundary condition is satisfied. For the minimum value, $\partial\Pi^* \ \partial q=0$, the resulting equation can be written as

$$K^*q = F^* \tag{13}$$

where $K^*=K+SC^TC$, $F^*=F+SC^Td$.

For identical finite element model and boundary conditions, the result of the calculation is influenced by the parameter S in the penalty function. If S is large enough, the boundary conditions play a critical role and the adjustment will be only along the tangential direction of the vertices. Thus, depending on the size and precision of the model, a relatively large S is taken to guarantee the effectiveness of adjustment.

4.2.3 2D example by FEA-based method

Figure 14 illustrates the FEA-based mesh regularization method in a simplified 2D situation. The displacement boundary constraint is added to every vertex. The value of the displacement boundary constraint is manufacturing deviation, which has been simulated for every vertex, and the directions are vertex normals.

For a vertex with just one displacement boundary constraint, it can be adjusted along its local tangent direction. For a vertex on the edge, which is shown in the dashed circle region, this has two nonparallel displacement boundary constraints, and its position is fully constrained in 2D. When dealing with the generation of skin model shapes, a similar method is extended to a 3D situation.

5 Simulation and comparison

5.1 Model used for comparison

As the vertices and triangles on the boundary cause problems in combining features with form error, here, we use the model with four typical edges in mechanical parts to evaluate the simulation result. This model is shown in Fig. 15.

The model is initially discretized and segmented into seven features, with different colors given to distinguish the faces. The four edges, $e1$, $e2$, $e3$, and $e4$, represent the edges between acute angle, obtuse angle, right angle, and edge with two tangent faces, respectively.

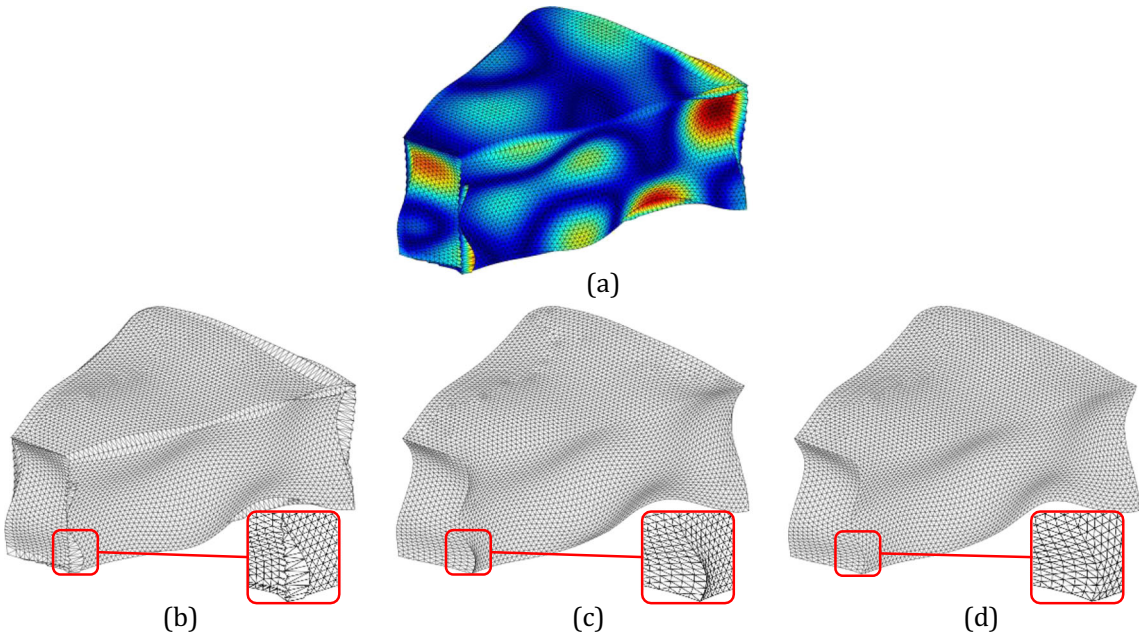

Fig. 16 **a** Direct deviation addition with color, **b** direct deviation addition, **c** Laplacian mesh regularization, **d** FEA-based regularization

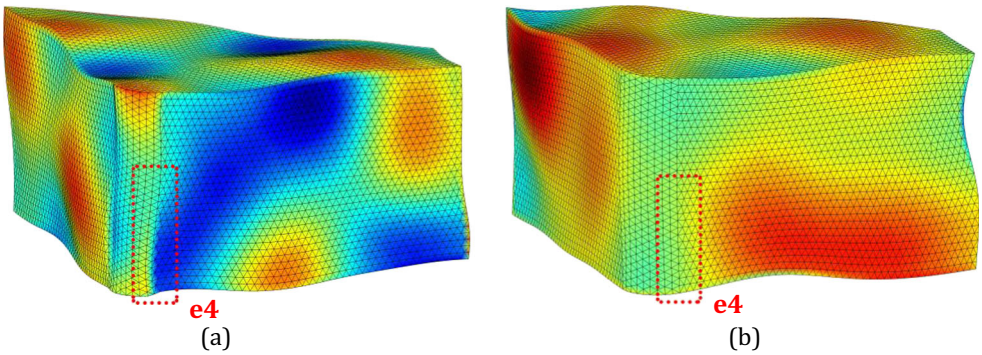

Fig. 17 Changes at tangent area *e*4. **a** Separated features, not continuous deviation. **b** Single feature, continuous deviation

5.2 Simulation results and comparison

To assess the effectiveness of different methods, we compare the simulation result by (1) the direct deviation addition method, (2) Laplacian mesh regularization, and (3) FEA-based mesh regularization. The form error for each feature is first simulated by the random field method, which has been introduced in earlier sections. To visualize the shape error of the model, the deviation is amplified. It should be noted that all three methods use the same result from the random field simulation, but differ in how the deviations are combined and adjusted.

As in the comparison method, deviations are assigned directly to the discrete skin model shape as shown in Fig. 16a, b. In Fig. 16a, the color denotes the simulation result from the random field method, while in Fig. 16b, the problems on the edges of the mesh are emphasized. It can be clearly seen that in Fig. 16b, the edges of the mesh have different degrees of stretch, compression, and intersection.

Figure 16c shows the result for the Laplacian mesh regularization. This is a local method and 200 iterations are conducted to smooth the mesh. With the proposed regularization strategy, the problems on the edges are eliminated, and the simulated manufacturing deviations are conserved. For this method, criteria are required (e.g., not contain mesh intersections, threshold value of smallest adjustment, etc.) to decide whether or not to continue the iterations.

The result for the FEA-based regularization method is given in Fig. 16d. As can be seen from the zoomed in areas, a more regular and smoother edge is generated compared to Fig. 16b, c, and only one linear problem needs to be solved. Considering its complexity and effectiveness, the FEA-based mesh regularization could be the best choice for our problem.

Based on the discussion above, by applying the adjustment with the FEA method, a reliable combination process could be conducted and the skin model shape is generated. However, one thing that should be considered is the connection of the tangent area, as shown in *e*4 of Fig. 15. When we separate the tangent connected features and assign manufacturing defects to them independently, dramatic changes may happen at the edge area, as in *e*4 in Fig. 17a. This is possible if the two tangent-connected features are machined in separate processes. If we machine them at the same time, a more continuous simulation result is preferred and we should regard the two connected features as one feature before simulation with the random field method. Figure 17b shows the result when the tangent features are considered together in simulation. Deviations of the tangent features are changing continuously. The decision to separate the two tangent features or not depends on the manufacturing process. Thus, to guarantee that the skin model shape represents realistic parts, it is better to keep the simulation process in accordance with the manufacturing process.

5.3 Application with mechanical part

The model we use for method comparison is a simple one, but it does contain several different types of edge situation. To verify

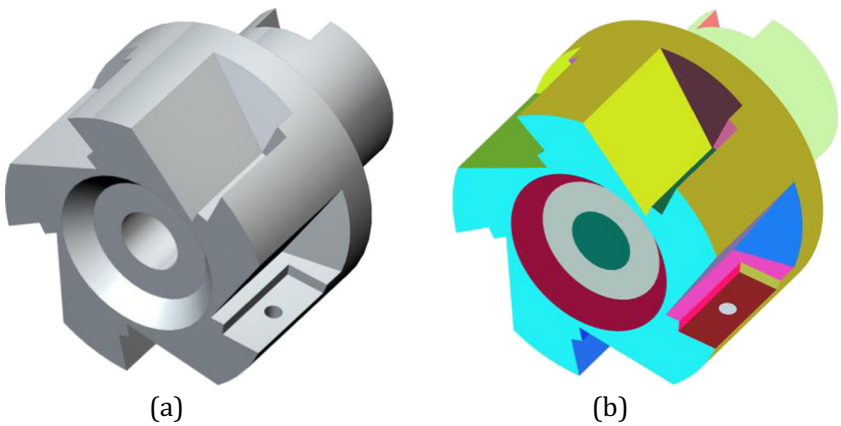

Fig. 18 Body of milling tool. **a** Nominal model. **b** Model after segmentation

the effectiveness of the proposed simulation procedure and deviation combination method, a representative mechanical part with complex shapes is used to generate its skin model shape.

The model we used here is a cutter body for milling. The nominal shape of the model is seen from Fig. 18a. Its surfaces are segmented into single features, which are distinguished by different colors in Fig. 18b. The modal-based simulation method is used to simulate manufacturing deviations. For each feature, four modes are chosen randomly and the maximum sum of the deviation could be 0.4.

The simulated deviations are amplified 15 times. In Fig. 19a–c, the simulated manufacturing deviations are added to the nominal model directly. Figure 19a aims at showing the global deviation shape in color, while Fig. 19b, c emphasizes local mesh problems. As shown in Fig. 19b, triangle meshes close to the corner and edge are heavily compressed. In the upper box of Fig. 19c, as the deviation values on vertices are larger than the mesh size of their neighboring triangles, self-intersection happens and shapes like sawtooth are generated on the edge. In the lower box of Fig. 19c, some triangles are compressed while others are stretched. Besides these four problems that have been pointed out, there are further problems if we check the model in detail.

Figure 19d, e shows the result by adding manufacturing deviations with the FEA-based global adjustment method.

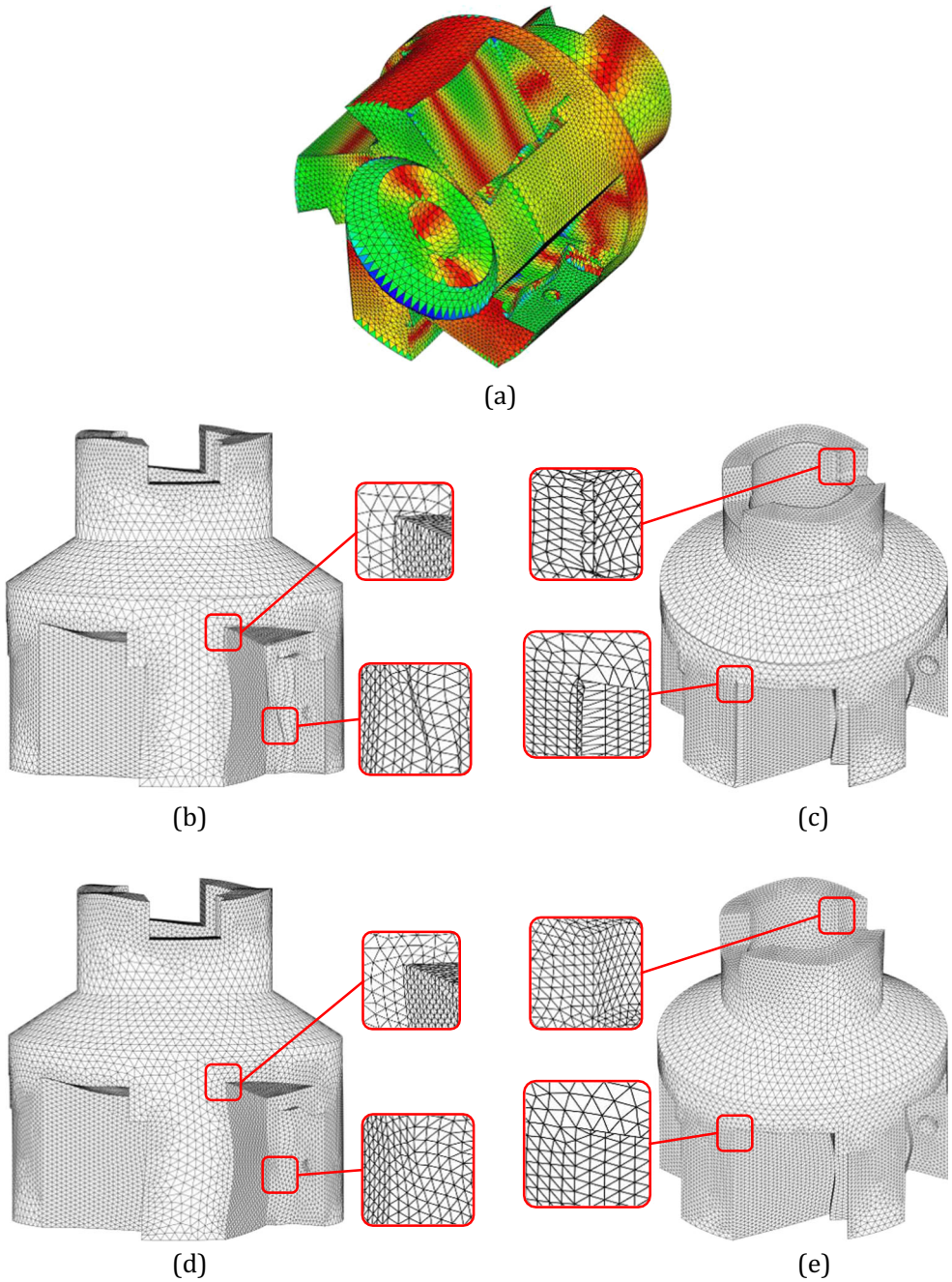

Fig. 19 Skin model shapes with simulated deviations. **a**–**c** Adding deviations to nominal model directly. **d**, **e** Adding deviations to nominal model by FEA-based method

The same places are zoomed in to show the effectiveness of the method. It can be clearly seen that after adjustment, meshes close to the edge are more equally distributed, while the shapes of the geometry (original edges and the simulated manufacturing deviations) are conserved.

6 Conclusion

The objective of this article is to present different approaches to generating consistent skin model shapes, so they can be used in tolerancing, manufacturing, and metrology. Geometrical problems during skin model shape simulation (self-intersection, increase of the deviation, etc.) are given and analyzed. Two solutions are proposed to solve these problems, the local method and the global method.

Local methods, like Laplacian mesh smoothing or spring analogy-based mesh adjustment, are used to regularize meshes at the edges. Due to local properties, iterative calculation, and the need for stop criteria, they are not the best choice for us.

A global method based on FEA is then introduced to generate skin model shapes while avoiding the drawbacks of local methods. In the FEA-based method, the manufacturing deviations of each feature are considered as displacement boundary conditions. With the penalty function approach, the combination of manufacturing deviations and the adjustment of mesh (to solve geometrical problems) could be done within a single global calculation without iterations. Comparisons between local and global methods are conducted, and the FEA-based global method generates better results than local methods.

Based on the simulation procedure and methods we have proposed, consistent skin model shapes could be generated. However, the generation of skin model shapes is only the first step, and more research efforts are needed for further promising applications, such as tolerance analysis, virtual metrology, and deviation visualization.

Compliance with ethical standards

Funding This work was supported by the China Scholarship Council.

Reference

1. Chen H, Jin S, Li Z, Lai X (2014) A comprehensive study of three dimensional tolerance analysis methods. Comput Aided Des 53:1–13. doi:10.1016/j.cad.2014.02.014
2. Ameta G, Serge S, Giordano M (2011) Comparison of spatial math models for tolerance analysis: tolerance-maps, deviation domain, and TTRS. J Comput Inf Sci Eng 11:21004
3. Requicha AAG (1983) Toward a theory of geometric tolerancing. Int J Robot Res 2:45–60. doi:10.1177/027836498300200403
4. Wirtz A (1993) Vectorial tolerancing: a basic element for quality control. 3rd CIRP
5. Geis A, Husung S, Oberänder A et al (2015) Use of vectorial tolerances for direct representation and analysis in CAD-systems. Procedia CIRP 27:230–240. doi:10.1016/j.procir.2015.04.071
6. Desrochers A, Clément A (1994) A dimensioning and tolerancing assistance model for CAD/CAM systems. Int J Adv Manuf Technol 9:352–361
7. Clément A, Desrochers A, Riviere A (1991) Theory and Practice of 3-D Tolerancing for Assembly. École de technologie supérieure
8. Teissandier D, Couetard Y, Gérard A (1999) A computer aided tolerancing model: proportioned assembly clearance volume. Comput Aided Des 31:805–817
9. Teissandier D, Couetard Y, Delos V (1999) Operations on polytopes: application to tolerance analysis. Glob. Consistency Toler. Springer, In, pp 425–434
10. Davidson JK, Mujezinović A, Shah JJ (2002) A new mathematical model for geometric tolerances as applied to round faces. J Mech Des 124:609. doi:10.1115/1.1497362
11. Schleich B, Anwer N, Zhu Z, et al (2014) Comparative Study on Tolerance Analysis Approaches. Int. Symp. Robust Des. ISoRD14
12. Mathieu L, Ballu A (2007) A model for a coherent and complete tolerancing process. In: Davidson JK (ed) Models Comput. Aided Toler. Des. Manuf. Springer Netherlands, Dordrecht, pp 35–44
13. Ballu A, Mathieu L, Dantan J-Y (2015) Formal language for GeoSpelling. J Comput Inf Sci Eng 15:21009. doi:10.1115/1.4029216
14. Hu YZ, Tonder K (1992) Simulation of 3-D random rough surface by 2-D digital filter and fourier analysis. Int J Mach Tools Manuf 32:83–90. doi:10.1016/0890-6955(92)90064-N
15. Yastrebov VA, Anciaux G, Molinari J-F (2015) From infinitesimal to full contact between rough surfaces: evolution of the contact area. Int J Solids Struct 52:83–102. doi:10.1016/j.ijsolstr.2014.09.019
16. Wilma P, Giovanni M (2015) Manufacturing signature for tolerance analysis. J Comput Inf Sci Eng 15:21005
17. Yanlong C, Bo L, Xuefeng Y et al (2015) Geometrical simulation of multiscale Toleranced surface with consideration of the tolerancing principle. J Comput Inf Sci Eng 15:21006
18. Franciosa P, Gerbino S, Patalano S (2011) Simulation of variational compliant assemblies with shape errors based on morphing mesh approach. Int J Adv Manuf Technol 53:47–61. doi:10.1007/s00170-010-2839-4
19. Huang W, Kong Z (2008) Simulation and integration of geometric and rigid body kinematics errors for assembly variation analysis. J Manuf Syst 27:36–44. doi:10.1016/j.jmsy.2008.06.004
20. Ballu A, Mathieu L (1996) Univocal expression of functional and geometrical tolerances for design, manufacturing and inspection. In: Kimura F (ed) Comput.-aided Toler. Springer Netherlands, Dordrecht, pp 31–46
21. ISO 17450–1:2011 Geometric product specification—general concepts—part 1: model for geometrical specification and verification
22. Anwer N, Ballu A, Mathieu L (2013) The skin model, a comprehensive geometric model for engineering design. CIRP Ann-Manuf Technol 62:143–146
23. Schleich B, Anwer N, Mathieu L, Wartzack S (2014) Skin model shapes: a new paradigm shift for geometric variations modelling in mechanical engineering. Comput Aided Des 50:1–15. doi:10.1016/j.cad.2014.01.001
24. Zhang M, Anwer N, Stockinger A et al (2013) Discrete shape modeling for skin model representation. Proc Inst Mech Eng Part B J Eng Manuf 227:672–680. doi:10.1177/0954405412466987
25. Henke RP, Summerhays KD, Baldwin JM et al (1999) Methods for evaluation of systematic geometric deviations in machined parts and their relationships to process variables. Precis Eng 23:273–292
26. Schleich B, Wartzack S, Anwer N, Mathieu L (2015) Skin model shapes: offering new potentials for modelling product shape variability. In: ASME 2015 Int. Des. Eng. Tech. Conf. Comput. Inf. Eng. Conf. American Society of Mechanical Engineers, p V01AT02A015–V01AT02A015

27. Wang H, Li G, Zhong Z (2008) Optimization of sheet metal forming processes by adaptive response surface based on intelligent sampling method. J Mater Process Technol 197:77–88. doi:10.1016/j.jmatprotec.2007.06.018
28. Hu M, Lin Z, Lai X, Ni J (2001) Simulation and analysis of assembly processes considering compliant, non-ideal parts and tooling variations. Int J Mach Tools Manuf 41:2233–2243
29. Blackmore D, Leu M, Wang LP (1997) The sweep-envelope differential equation algorithm and its application to NC machining verification. Comput Aided Des 29:629–637. doi:10.1016/S0010-4485(96)00101-7
30. Lee S-K, Ko S-L (2002) Development of simulation system for machining process using enhanced Z map model. J Mater Process Technol 130:608–617
31. Lin Y, Shen Y-L (2004) Enhanced virtual machining for sculptured surfaces by integrating machine tool error models into NC machining simulation. Int J Mach Tools Manuf 44:79–86. doi:10.1016/j.ijmachtools.2003.08.003
32. Movahhedy M, Gadala MS, Altintas Y (2000) Simulation of the orthogonal metal cutting process using an arbitrary Lagrangian–Eulerian finite-element method. J Mater Process Technol 103:267–275
33. Soori M, Arezoo B, Habibi M (2014) Virtual machining considering dimensional, geometrical and tool deflection errors in three-axis CNC milling machines. J Manuf Syst 33:498–507. doi:10.1016/j.jmsy.2014.04.007
34. Spence AD, Abrari F, Elbestawi MA (2000) Integrated solid modeller based solutions for machining. Comput Aided Des 32:553–568. doi:10.1016/S0010-4485(00)00042-7
35. Altintas Y, Kersting P, Biermann D et al (2014) Virtual process systems for part machining operations. CIRP Ann - Manuf Technol 63:585–605. doi:10.1016/j.cirp.2014.05.007
36. Zhang M, Anwer N, Mathieu L, Zhao H (2011) A discrete geometry framework for geometrical product specifications. Proc. 21st CIRP Des. Conf. Kaist MK Thompson Ed Pap
37. Wagersten O, Lindau B, Lindkvist L, Söderberg R (2014) Using morphing techniques in early variation analysis. J Comput Inf Sci Eng 14:11007
38. Das A, Franciosa P, Williams D, Ceglarek D (2016) Physics-driven shape variation modelling at early design stage. Procedia CIRP 41:1072–1077. doi:10.1016/j.procir.2016.01.031
39. Formosa F, Samper S (2007) Modal expression of form defects. In: Models Comput. Aided Toler, Des. Manuf. Springer, pp 13–22
40. Kingslake R, Shannon RR (1992) Basic wavefront aberration theory for optical metrology. Appl. Opt. Opt. Eng. Vol 11
41. Yan X, Ballu A (2016) Toward an automatic generation of part models with form error. Procedia CIRP 43:23–28. doi:10.1016/j.procir.2016.02.109
42. Jin S, Lewis RR, West D (2005) A comparison of algorithms for vertex normal computation. Vis Comput 21:71–82. doi:10.1007/s00371-004-0271-1
43. Chen C-Y, Cheng K-Y (2008) A sharpness-dependent filter for recovering sharp features in repaired 3D mesh models. Vis Comput Graph IEEE Trans On 14:200–212
44. Ju T (2009) Fixing geometric errors on polygonal models: a survey. J Comput Sci Technol 24:19–29
45. Yang L, Yan Q, Xiao C (2016) Shape-controllable geometry completion for point cloud models. Vis Comput. doi:10.1007/s00371-016-1208-1
46. Ballu A, Yan X, Blanchard A et al (2016) Virtual metrology laboratory for e-learning. Procedia CIRP 43:148–153. doi:10.1016/j.procir.2016.02.110
47. Ohtake Y, Belyaev A, Bogaevski I (2001) Mesh regularization and adaptive smoothing. Comput Aided Des 33:789–800. doi:10.1016/S0010-4485(01)00095-1
48. Riehl S, Steinmann P (2015) A staggered approach to shape and topology optimization using the traction method and an evolutionary-type advancing front algorithm. Comput Methods Appl Mech Eng 287:1–30. doi:10.1016/j.cma.2015.01.007
49. Yamauchi H, Lee S, Lee Y, et al (2005) Feature sensitive mesh segmentation with mean shift. In: Shape Model. Appl. 2005 Int. Conf. IEEE, pp 236–243
50. Kobbelt L, Campagna S, Vorsatz J, Seidel H-P (1998) Interactive multi-resolution modeling on arbitrary meshes. In: Proc. 25th Annu. Conf. Comput. Graph. Interact. Tech. ACM, pp 105–114
51. Ait-Ali-Yahia D, Baruzzi G, Habashi WG et al (2002) Anisotropic mesh adaptation: towards user-independent, mesh-independent and solver-independent CFD. Part II. Structured grids. Int J Numer Methods Fluids 39:657–673
52. Blom FJ (2000) Considerations on the spring analogy. Int J Numer Methods Fluids 32:647–668. doi:10.1002/(SICI)1097-0363(20000330)32:6<647::AID-FLD979>3.0.CO;2-K
53. Zeng D, Ethier CR (2005) A semi-torsional spring analogy model for updating unstructured meshes in 3D moving domains. Finite Elem Anal Des 41:1118–1139. doi:10.1016/j.finel.2005.01.003
54. Amirante D, Hills NJ, Barnes CJ (2012) A moving mesh algorithm for aero-thermo-mechanical modelling in turbomachinery. Int J Numer Methods Fluids 70:1118–1138
55. Hsu S-Y, Chang C-L (2007) Mesh deformation based on fully stressed design: the method and 2-D examples. Int J Numer Methods Eng 72:606–629
56. Zienkiewicz OC, Taylor RL, Zienkiewicz OC, Taylor RL (1977) The finite element method. McGraw-hill London
57. Zeng P (2007) Fundamentals of finite element analysis. Tsinghua University Press, Beijing